5th International Conference on Multiphase Flow, ICMF'04
Yokohama, Japan, May 30–June 4, 2004
Paper No. 392

s

The Favre Averaged Drag Model for Turbulent Dispersion in Eulerian Multi-Phase Flows

Alan D. Burns[1], Thomas Frank[2], Ian Hamill[3], and Jun-Mei Shi[4]

1: ANSYS CFX, The Gemini Building, Fermi Avenue, Didcot, OX11 0QR, UK, alan.burns@ansys.com
2: ANSYS CFX Germany, Staudenfeldweg 12, 83624 Otterfing, Germany, thomas.frank@ansys.com
3: ANSYS CFX, The Gemini Building, Fermi Avenue, Didcot, OX11 0QR, UK, ian.hamill@ansys.com
4: Forschungszentrum Rossendorf, Bautzner Landstrasse 129, 01328 Dresden, Germany, j.shi@fz-rossendorf.de

Abstract. A general framework is presented for the modeling of turbulent dispersion in Eulerian Multi-Phase Flows. The approach is based on a double averaging procedure of the local instant equations.

We start with the ensemble averaged equations of Eulerian multi-phase flow. We perform a second time average of these, in order to form equations which may be used to model turbulent multi-phase flows. These are conveniently expressed in terms of Favre or Mass averaged variables.

Turbulent dispersion is modeled by performing a time average of the interphase drag term in its modeled form, and expressing it in terms of Favre averaged variables. The resulting double averaged momentum equations contain additional terms which account for a turbulent dispersion force. We call the resulting model the Favre Averaged Drag (FAD) model for turbulent dispersion. It is first presented in a general form which may be used in conjunction with any Reynolds averaged turbulence model, and for an arbitrary number of phases with arbitrary morphologies.

For the purposes of this study, we make two further specializations, to poly-dispersed multiphase flows, and to turbulence models which employ the eddy diffusivity hypothesis. The resulting model is compared to several other models that have appeared in the literature, We show that all are special cases of the FAD model, within certain physical and mathematical limitations. Hence the FAD model encompasses all of these models, but has a potentially wider range of universality.

The FAD model has been implemented in the commercial CFD package, CFX-5, and tested against a range of dispersed multiphase flows, including bubbly flows in vertical pipes, and liquid-solid flows in mixing vessels. The FAD model is shown to yield superior predictions in all cases.

1. Introduction

The accurate modeling of multi-dimensional turbulent multiphase flows is a challenging task. Many phenomena occur which need to be accounted for explicitly in the modeling procedure. For example:

Turbulent Dispersion. Turbulence in one phase has a direct effect on the migration of fluid particles in the other phases. For example, in a dispersed multi-phase flow, turbulence in the continuous phase causes particles in the dispersed phase to be transported from regions of high concentration to regions of low concentration.

Turbulence Modulation. Conversely, the mere presence of dispersed phases within a continuous phase can affect turbulence within the continuous phase. Large particles tend to increase turbulence levels in the continuous phase, due to enhance shear production in their wakes. However, large concentrations of small particles tend to decrease turbulence in the continuous phase. See, for example, Crowe (2000).

Buoyancy Production. Large mean density gradients are the rule rather than the exception in most practical multi-phase flows. Hence, buoyancy effects on turbulent production should be

expected to be important. For example, significant damping of turbulence should be expected to occur in stably stratified multi-phase flows.

In this paper, we address the phenomenon of turbulent dispersion. However, we expect the methods used here to also have significant impact on future modeling of other turbulent multi-phase flow phenomena.

2. Averaging Procedures

Averaging procedures are traditionally used in the modeling of both single-phase turbulent flows, and multi-phase flows.

2.1 Single Phase Turbulent Flow

Typically, the unaveraged Navier-Stokes equations are time- or ensemble-averaged to form the Reynolds Averaged Navier-Stokes equations. In particular, averaging of the non-linear advection term produces an additional contribution to the momentum flux, known as the Reynolds Stress tensor. The equations are closed by providing closure models for the Reynolds stresses. The simplest models employ the eddy viscosity hypothesis. More complex second order closure models solve modeled transport equations for the Reynolds Stresses.

For variable density single-phase flows, it turns out to be convenient to express the time- or ensemble-average equations in terms of Favre or Mass Weighted variables. The advantages of this formulation are:

1. There are no additional terms in the averaged continuity equation.

2. There are fewer terms requiring direct modeling in the momentum and other transport equations.

2.2 Eulerian Multi Phase Flow.

We start with the local instant transport equations which govern the flow of each distinct phase. These are the time-dependent Navier-Stokes Equations:

$$\frac{\partial}{\partial t}(\rho U_k)+\frac{\partial}{\partial x_i}(\rho U_i U_k-\tau_{ik})=-\frac{\partial P}{\partial x_k}+B_k \qquad (1)$$

$$\frac{\partial}{\partial t}(\rho)+\frac{\partial}{\partial x_i}(\rho U_i)=0 \qquad (2)$$

Here, ρ, U_i denote the local density and velocity fields, τ_{ij} denotes the viscous stress tensor, and P and B_k denote pressure and volumetric body forces. At any point in space and time, only one phase may be present. We denote distinct phases with Greek subscripts α, β etc. For each phase, we define the phase indicator function, or characteristic function:

$$\chi_\alpha(x,t)=1 \text{ if phase } \alpha \text{ is present, } \chi_\alpha(x,t)=0 \text{ otherwise.}$$

We select an appropriate averaging procedure, namely ensemble-, time- or space-averaging, $\Phi \to \langle \Phi \rangle$ and we define phase-averaged variables as follows:

$$r_\alpha = \langle \chi_\alpha \rangle = \text{volume fraction of phase } \alpha \qquad (3)$$

$$\rho_\alpha = \langle \chi_\alpha \rho \rangle / r_\alpha = \text{material density of phase } \alpha \qquad (4)$$

$$\Phi_\alpha = \langle \chi_\alpha \rho \Phi \rangle / \rho_\alpha = \text{phase averaged transport variable in phase } \alpha \qquad (5)$$

Here, Φ denotes any transported variable, and we note that the phase averaging procedure is a mass-weighted averaging procedure. Strictly speaking, r_α is only a volume fraction if we are employing volume averaging. It is a residence time average if time averaging, and an average fraction of occurrence if ensemble averaging.

Phase averaged equations are derived by multiplying the local instant equations by the phase indicator functions, and averaging. Two distinct approaches are predominant in the literature:

1. Take single-phase flow equations in each phase separately, supplemented by interphase boundary conditions, or jump conditions. See Drew 1983 for details.

2. Alternatively, use the local instant equations defined in the whole of space, using the theory of distributions to permit partial derivatives of discontinuous quantities to be defined. This is the approach of Kataoka (1986) and Kataoka and Serizawa (1989). It is conceptually simpler in that it does not require detailed accounting of interphase boundary conditions.

Both approaches lead to phase averaged equations which typically take the form:

$$\frac{\partial}{\partial t}\left(r_\alpha \rho_\alpha U_{\alpha k}\right) + \frac{\partial}{\partial x_i}\left(r_\alpha\left(\rho_\alpha U_{\alpha i} U_{\alpha k} - \left(\tau_{\alpha i k} + \tau^t_{\alpha i k}\right)\right)\right) = -r_\alpha \frac{\partial P}{\partial x_k} + r_\alpha B_k + M_{\alpha k} \tag{6}$$

$$\frac{\partial}{\partial t}\left(r_\alpha \rho_\alpha\right) + \frac{\partial}{\partial x_i}\left(r_\alpha \rho_\alpha U_{\alpha i}\right) = 0 \tag{7}$$

Note that $M_{\alpha k}$ denotes the interfacial forces acting on phase α due to the presence of other phases. This is traditionally split into several contributions from drag force, lift force, virtual mass force etc. Also, $\tau^t_{\alpha i k}$ denote Reynolds stress like terms,

$$\tau^t_{\alpha i k} = -\rho_\alpha \left\langle u'_{i\alpha} u'_{j\alpha} \right\rangle \tag{8}$$

where $u'_{i\alpha}$ denote fluctuating velocity fields relative to the phase average.

2.3 Turbulent Multi Phase Flow.

The phase averaged equations (6) and (7) are already derived using an averaging procedure. Moreover, they contain Reynolds stress like terms (8). Hence, it is not unreasonable to assume that they provide a complete basis for the modeling of turbulent multi-phase flow. This approach has been followed, for example, by Kashiwa and VanderHeyden (2000). Kataoka and Serizawa (1989) derived exact transport equations for the phase averaged turbulent kinetic energy and energy dissipation which arise in this approach. In particular, terms may be identified for enhanced turbulence production, which are exact once the terms for interfacial forces are closed. Attempts have also been made to model enhanced turbulence dissipation based on this approach (Serizawa and Kataoka 1990).

However, if the phase averaged equations are derived using *ensemble* averaging, then they are fully space and time dependent. Hence, it makes mathematical sense to apply a second *time-averaging* operation to the equations, and to use the resulting *double averaged* equations as the basis for modeling turbulent multi-phase flows. This approach has also been followed by many authors, for example, Elghobashi and Abou-Arab (1983), Besnard and Harlow (1988).

It is not obvious to the present authors which of the above two approaches is more soundly based physically. We believe it is important to work out the consequences of both approaches, and to compare resulting models with experiment. In particular, we shall see that the double averaging approach leads to some nice physically intuitive models of turbulent multi-phase phenomena, which we believe are difficult to derive from the single averaging approach alone.

Within the double averaging approach, there is a further choice to be made. Namely, whether to base the modeled equations on time averaged or on Favre averaged variables. Experience with single phase turbulent flow has demonstrated the superiority of the Favre averaged approach for variable density flows, as it leads to much fewer higher order correlation terms which require modeling. As multiphase flows have much in common with variable density single phase flows, we expect the same principles to apply. Elghobashi and Abou-Arab

(1983) derived time-averaged versions of the phase-averaged equations, including exact transport equations for turbulent kinetic energy and dissipation. These contained 38 and 64 terms respectively. Besnard and Harlow (1988) employed the Favre averaging approach.

2.4 Favre Averaging.

Favre averaging of phase-averaged variables is defined as follows:

$$\tilde{\Phi}_\alpha = \overline{r_\alpha \rho_\alpha \Phi_\alpha} / \overline{r_\alpha \rho_\alpha} \tag{9}$$

Here, the phase averaged variables are as defined in equations (3), (4) and (5), and the overbar denotes the time averaging operation. For simplicity, we consider constant density phases, in which case Favre averaging reduces to a volume fraction weighted average:

$$\tilde{\Phi}_\alpha = \overline{r_\alpha \Phi_\alpha} / \overline{r_\alpha} \qquad \Rightarrow \qquad \overline{r_\alpha \Phi_\alpha} = \overline{r_\alpha} \tilde{\Phi}_\alpha \tag{10}$$

From this, we deduce a simple relationship between Favre-averaged and time-averaged quantities:

$$\overline{r_\alpha \Phi_\alpha} = \overline{\left(\overline{r_\alpha} + r'_\alpha\right)\left(\overline{\Phi_\alpha} + \phi'_\alpha\right)} \qquad \Rightarrow \qquad \tilde{\Phi}_\alpha = \overline{\Phi_\alpha} + \overline{r'_\alpha \phi'}_\alpha / \overline{r_\alpha} \tag{11}$$

Here, single dashes denote fluctuating quantities relative to the time-averaged variable. This indicates the importance of correlations between fluctuating volume fractions and fluctuating variables to relate Favre averaged and time-averaged variables.

In particular, time-averaged and Favre averaged velocities are related by:

$$\tilde{\vec{U}}_\alpha = \overline{\vec{U}}_\alpha + \overline{\vec{u}''_\alpha} \quad , \qquad \overline{\vec{u}''_\alpha} = \overline{r'_\alpha \vec{u}'_\alpha} / \overline{r_\alpha} \tag{12}$$

The quantity $\overline{r'_\alpha \vec{u}'_\alpha}$ is fundamental to turbulent dispersion, as it describes how phasic volume fractions are spread out by velocity fluctuations. In eddy-viscosity type turbulence models, it is modeled via the eddy diffusivity hypothesis (EDH):

$$\overline{r'_\alpha \vec{u}'_\alpha} = -\frac{\nu_{t\alpha}}{\sigma_{r\alpha}} \nabla \overline{r_\alpha} \tag{13}$$

Here, $\nu_{t\alpha}$ is the kinematic eddy viscosity of phase α, and $\sigma_{r\alpha}$ is the turbulent Prandtl number for volume fraction dispersion, expected to be of order unity.

2.5 Favre Averaged Continuity Equations.

Time averaging the phasic continuity equations (7) gives:

$$\frac{\partial}{\partial t}\left(\rho_\alpha \overline{r_\alpha}\right) + \frac{\partial}{\partial x_i}\left(\rho_\alpha \left(\overline{r_\alpha U_{i\alpha}} + \overline{r_\alpha u'_{i\alpha}}\right)\right) = 0 \tag{14}$$

Hence, we have an extra term involving the volume fraction-velocity correlation. This yields an additional diffusion term if we employ the eddy diffusivity hypothesis (13).

However, we may use the relation (10) to express the time-averaged continuity equations in terms of Favre averaged velocities:

$$\frac{\partial}{\partial t}\left(\rho_\alpha \overline{r_\alpha}\right) + \frac{\partial}{\partial x_i}\left(\rho_\alpha \overline{r_\alpha} \tilde{U}_{i\alpha}\right) = 0 \tag{15}$$

In this case, no extra terms appear. This is clearly a mathematical simplification, not a physical one. We shall see in the next section that, using Favre averaging, turbulent dispersion may be accounted for entirely in the time-averaged momentum equations.

3. Turbulent Dispersion Force

Consider the concrete situation of a turbulent continuous phase interacting with a dispersed particulate phase. Particles will tend to get caught up in continuous phase turbulent eddies, and hence be carried from regions of high concentration to regions of low concentration.

The mechanism responsible for particle acceleration due to continuous phase velocity fluctuations is that of interphase momentum transfer. That is, the interfacial forces $M_{\alpha k}$ occurring in the phase averaged momentum equations (6). Hence, it is reasonable to assume that turbulent dispersion may be modeled using the time average of the fluctuating part of the interphase momentum force. This idea was first introduced by Gosman et al (1992), employing the drag component only of the total interfacial force. The paper by Behzadi et al (2001) subsequently considered the additional effects of the lift and virtual mass forces, but found them not to be significant.

We restrict our attention here to the interphase drag force. We assume a general model for this force which is proportional to the slip velocity and the interfacial area density $A_{\alpha\beta}$:

$$\vec{M}_\alpha = C_{\alpha\beta}\left(\vec{U}_\beta - \vec{U}_\alpha\right) = D_{\alpha\beta}A_{\alpha\beta}\left(\vec{U}_\beta - \vec{U}_\alpha\right) \tag{16}$$

For example, for a dispersed two phase flow involving a continuous phase α, and dispersed phase β, with Sauter mean diameter d_β and non-dimensional drag coefficient C_D, we have:

$$C_{\alpha\beta} = \frac{3}{4}C_D\frac{r_\beta\rho_\alpha}{d_\beta}\left|\vec{U}_\beta - \vec{U}_\alpha\right| = \frac{1}{8}C_D A_{\alpha\beta}\rho_\alpha\left|\vec{U}_\beta - \vec{U}_\alpha\right|, \qquad A_{\alpha\beta} = \frac{6r_\beta}{d_\beta} \tag{17}$$

As a first approximation, we assume that the proportionality factor $D_{\alpha\beta}$ in equation (16) may be treated as approximately constant as far as the averaging procedure is concerned. That is, we only account for velocity fluctuations in the linear slip velocity term, and for volume fraction fluctuations in the area density term. This will be true for dispersed two phase flows whose drag coefficient obeys Stokes' law, but it is an approximation for other drag laws. This approximation may be relaxed in further work.

3.1 Time Averaged Drag Force

Time average equation (16), taking into account velocity fluctuations and area density fluctuations. We obtain:

$$\overline{\vec{M}_\alpha} = D_{\alpha\beta}\left(\overline{A_{\alpha\beta}}\left(\overline{\vec{U}_\beta} - \overline{\vec{U}_\alpha}\right) + \overline{a'_{\alpha\beta}\left(\vec{u}'_\beta - \vec{u}'\right)}\right) \tag{18}$$

So, in this case, the time-averaged drag term consists of the original unaveraged drag term, written in terms of time-averaged variables, plus an extra term proportional to the area density-slip-velocity correlation $D_{\alpha\beta}\left(\overline{a'_{\alpha\beta}\left(\vec{u}'_\beta - \vec{u}'_\alpha\right)}\right)$. If modeled using the eddy diffusivity hypothesis, this is given by:

$$D_{\alpha\beta}\left(\overline{a'_{\alpha\beta}\left(\vec{u}'_\beta - \vec{u}'_\alpha\right)}\right) = -\overline{C_{\alpha\beta}}\left(\frac{\nu_{t\beta}}{\sigma_{A\beta}} - \frac{\nu_{t\alpha}}{\sigma_{A\alpha}}\right)\frac{\nabla\overline{A_{\alpha\beta}}}{\overline{A_{\alpha\beta}}} \tag{19}$$

where $\sigma_{A\alpha}$ and $\sigma_{A\beta}$ are turbulent Prandtl numbers for interfacial area density.

3.2 Favre Averaged Drag Force

We may express the time averaged drag (18) in terms of Favre averaged velocities using the relation (12). We obtain:

$$\overline{\vec{M}_\alpha} = C_{\alpha\beta}\left(\tilde{U}_\beta - \tilde{U}_\alpha\right) + \vec{M}_\alpha^{TD} \tag{20}$$

This contains the original drag force, expressed in terms of Favre averaged velocities, together with an additional term which is given by:

Turbulent Dispersion Force (General Form):

$$\vec{M}_\alpha^{TD} = -\vec{M}_\beta^{TD} = -\overline{C_{\alpha\beta}}\left(\frac{\overline{r'_\beta \vec{u}'_\beta}}{\overline{r_\beta}} - \frac{\overline{r'_\alpha \vec{u}'_\alpha}}{\overline{r_\alpha}} - \frac{\overline{a'_{\alpha\beta}\left(\vec{u}'_\beta - \vec{u}'_\alpha\right)}}{\overline{A_{\alpha\beta}}} \right) \tag{21}$$

If using the eddy diffusivity hypothesis (EDH), this may be closed as follows:

Modeled Form (EDH):

$$\vec{M}_\alpha^{TD} = -\vec{M}_\beta^{TD} = \overline{C_{\alpha\beta}}\left(\frac{\nu_{t\beta}}{\sigma_{r\beta}} \frac{\nabla \overline{r_\beta}}{\overline{r_\beta}} - \frac{\nu_{t\alpha}}{\sigma_{r\alpha}} \frac{\nabla \overline{r_\alpha}}{\overline{r_\alpha}} - \left(\frac{\nu_{t\beta}}{\sigma_{A\beta}} - \frac{\nu_{t\alpha}}{\sigma_{A\alpha}} \right) \frac{\nabla \overline{A_{\alpha\beta}}}{\overline{A_{\alpha\beta}}} \right) \tag{22}$$

It is expected that all turbulent Prandlt numbers should be of order unity.

3.3 Poly-Dispersed Multi-Phase Flow

Equation (21) expresses the most general form of the Favre Averaged Drag (FAD) model for the turbulent dispersion force. It is applicable to first and second moment closure turbulence models, and to phase pairs of arbitrary morphology. We now wish to restrict attention to dispersed multi-phase flows, in which case further simplifications are obtained.

Assume throughout that phase α represents a continuous phase, and that phase β represents a dispersed phase of mean diameter d_β. Then, the interfacial area density is given by:

$$A_{\alpha\beta} = \frac{6 r_\beta}{d_\beta} \tag{23}$$

Hence, the area density-slip-velocity correlation may be expressed in terms of volume fraction-velocity correlations:

$$\frac{\overline{a'_{\alpha\beta}\left(\vec{u}'_\beta - \vec{u}'_\alpha\right)}}{\overline{A_{\alpha\beta}}} = \frac{\overline{r'_\beta\left(\vec{u}'_\beta - \vec{u}'_\alpha\right)}}{\overline{r_\beta}} \tag{24}$$

Consequently, equations (21) and (22) further simplify to:

General Form

$$\vec{M}_\alpha^{TD} = -\vec{M}_\beta^{TD} = \overline{C_{\alpha\beta}}\left(\frac{\overline{r'_\alpha \vec{u}'_\alpha}}{\overline{r_\alpha}} - \frac{\overline{r'_\beta \vec{u}_\alpha}}{\overline{r_\beta}} \right) \tag{25}$$

Modeled Form (EDH):

$$\vec{M}_\alpha^{TD} = -\vec{M}_\beta^{TD} = \overline{C_{\alpha\beta}} \frac{\nu_{t\alpha}}{\sigma_{r\alpha}} \left(\frac{\nabla \overline{r_\beta}}{\overline{r_\beta}} - \frac{\nabla \overline{r_\alpha}}{\overline{r_\alpha}} \right) \tag{26}$$

It is interesting to note that all term involving the dispersed phase eddy viscosity have cancelled, so the modeled form of the turbulent dissipation force depends only on the continuous phase eddy viscosity. This cancellation occurs due to our inclusion of fluctuating area density effects.

3.4 Dispersed Two Phase Flow

In the special case of two phases only, $r_\alpha + r_\beta = 1$, so $\nabla \overline{r_\alpha} + \nabla \overline{r_\beta} = 0$. Hence, the modeled EDH form of the turbulent dispersion force reduces to a simple volume fraction gradient:

$$\vec{M}_\alpha^{TD} = -\vec{M}_\beta^{TD} = -\overline{C_{\alpha\beta}} \frac{\nu_{t\alpha}}{\sigma_{r\alpha}} \left(\frac{1}{\overline{r_\alpha}} + \frac{1}{\overline{r_\beta}} \right) \nabla \overline{r_\alpha} \tag{27}$$

4. Comparison with Other Models

In this section, we compare the Favre Averaged Drag (FAD) model with similar models derived by other authors. We restrict attention to the model equations (26) and (27) for dispersed multiphase flows employing the eddy diffusivity hypothesis. For comparison purposes, substitute equation (17) into (27) to express the dispersed 2-phase FAD+EVM model in terms of non-dimensional drag coefficient:

$$\vec{M}_\alpha^{TD} = -\vec{M}_\beta^{TD} = -\frac{3}{4} C_D \frac{\bar{r}_\beta \rho_\alpha}{d_\beta} \left| \vec{U}_\beta - \vec{U}_\alpha \right| \frac{\nu_{t\alpha}}{\sigma_{r\alpha}} \left(\frac{1}{\bar{r}_\alpha} + \frac{1}{\bar{r}_\beta} \right) \nabla \bar{r}_\alpha \tag{28}$$

In the limit of dilute dispersed two-phase flow, $r_\beta \to 0$, this is asymptotically equivalent to:

$$\vec{M}_\alpha^{TD} = -\vec{M}_\beta^{TD} = -\frac{3}{4} C_D \frac{\bar{r}_\beta \rho_\alpha}{d_\beta} \left| \vec{U}_\beta - \vec{U}_\alpha \right| \frac{\nu_{t\alpha}}{\sigma_{r\alpha}} \nabla \bar{r}_\alpha \tag{29}$$

4.1 Imperial College Model

As indicated in section 3, the idea of modeling the turbulence dispersion force by Favre averaging the drag term was first proposed by Gosman et al (1992). Following the exposition in Behzadi et al (2001), the turbulent contribution of the drag force is modeled using:

$$\vec{M}_\alpha^{TD} = -B \overline{\vec{u}_\alpha''} \tag{30}$$

where $B = \frac{3}{4} C_D \frac{\bar{r}_\beta \rho_\alpha}{d_\beta} \left| \vec{U}_\beta - \vec{U}_\alpha \right|$ and $\overline{\vec{u}_\alpha''}$ is modeled as $\overline{\vec{u}_\alpha''} = \frac{\nu_{t\alpha}}{\sigma_{r\alpha}} \nabla \bar{r}_\alpha$. Hence,

$$\vec{M}_\alpha^{TD} = -\vec{M}_\beta^{TD} = -\frac{3}{4} C_D \frac{\bar{r}_\beta \rho_\alpha}{d_\beta} \left| \vec{U}_\beta - \vec{U}_\alpha \right| \frac{\nu_{t\alpha}}{\sigma_{r\alpha}} \frac{\nabla \bar{r}_\alpha}{\bar{r}_\alpha} \tag{31}$$

This is very similar to, though not identical to equation (28) for the FAD model. Both have the same asymptotic limit (29), as $r_\beta \to 0$, for dilute dispersed two phase flow.

4.2 Chalmers University Model

Ljus (2000) and Johanssen et al (2001) have derived and validated a similar model to equation (27) for dispersed two phase flow. However, their model requires highly unconventional volume fraction Prandtl numbers, of order 0.001, to achieve reasonable agreement with experiment. This is due to minor errors in their analysis, which are clarified here.

Ljus (2000) implicitly uses time-averaging, but neglects the resulting diffusion term in the time-averaged continuity equation (14) on the grounds that volume fraction variations are small. Only the additional term from time-averaged drag, equation (18), is modeled, employing a model of the form:

$$D_{\alpha\beta}\left(\overline{a'_{\alpha\beta}\left(\vec{u}'_\beta - \vec{u}'_\alpha\right)}\right) = \beta_1 \nabla \bar{r}_\beta + \beta_2 \nabla k_\alpha \tag{32}$$

$$\beta_1 = \frac{\overline{C_{\alpha\beta}}}{\bar{r}_\beta} \frac{\nu_{t\beta}}{\sigma_{d1}} \qquad \beta_2 = \frac{\bar{r}_\beta \rho_\beta}{\sigma_{d1}} \tag{33}$$

The retention of volume fraction gradients in the first term means that their neglect in the continuity equation is incorrect. However, the model can be salvaged by reinterpreting the averaging procedure as Favre averaging, and taking the RHS of (32) as a model for the fluctuating terms in the Favre Averaged Drag, equation (21).

The unconventionally small volume fraction Prandtl numbers σ_{d1} arise because of the use of *dispersed* phase eddy viscosity in the definition of β_1. This is in contrast with our model equation (27) which only employs the *continuous* phase eddy viscosity. The Ljus model was

employed in conjunction with an algebraic model for dispersed phase eddy viscosity:

$$\nu_{t\beta} = \frac{\nu_{t\alpha}}{\sigma_{\nu\beta}} \tag{34}$$

Here, $\sigma_{\nu\beta}$ is an eddy viscosity Prandtl number, which is modeled as a function of the ratio of turbulent Stokes number, *St* = the ratio of particle relaxation time $\tau_{\beta,}$ and the integral turbulent time scale $\tau_{t,}$ as follows:

$$\sigma_{\nu\beta} = \frac{1}{1+St} \quad , \quad St = \frac{\tau_\beta}{\tau_t} \quad , \quad \tau_\beta = \frac{\overline{r_\beta}\rho_\alpha}{\overline{\overline{C_{\alpha\beta}}}} \quad , \quad \tau_t = 0.41\frac{k_\alpha}{\varepsilon_\alpha} \tag{35}$$

Hence, comparing the FAD model (27) with the first term of the Ljus model (32), we see that they are equivalent in the limit of small r_β, provided we make the algebraic identification:

$$\sigma_{d1} = \frac{\sigma_{r\alpha}}{\sigma_{\nu\beta}} \tag{36}$$

Thus, the parameter σ_{d1} in the Ljus model is not the true volume fraction Prandtl number. It is the ratio of the volume fraction Prandtl number and the eddy viscosity Prandtl number. This explains the unconventionally low value of σ_{d1} = 0.001 required to obtain agreement with experiment. The comparisons with experiment in Johansson et al (2001) involved large solid particles in gas, with large relaxation times, and hence correspondingly large values of the eddy viscosity Prandtl number $\sigma_{\nu\beta}$.

The second term of the Ljus model involves gradients of turbulent kinetic energy. Such terms are likely to occur in the FAD model if we were to take into account variations of $C_{\alpha\beta}$ which are linear in slip velocity. This may be a topic of future investigations.

4.3 RPI Models

Research workers at Rensselaer Polytechnic Institute (RPI) have developed two volume-fraction based gradient models for turbulent dispersion applied to bubbly two phase flows. These are both discussed below.

Lopez de Bertodano Model

The original model of Lopez de Bertodano (1992) takes the form:

$$\vec{M}_\alpha^{TD} = -\vec{M}_\beta^{TD} = -C_{TD}\rho_\alpha k_\alpha \nabla \overline{r_\alpha} \tag{37}$$

C_{TD} is a non-dimensional empirical constant. C_{TD} = 0.1 to 0.5 was found to give reasonable results for medium sized bubbles in the ellipsoidal particle regime (Lopez de Bertodano et al 1994a, 1994b). However, flow regimes involving very small bubbles or very small solid particles were found to require very different values of C_{TD}, up to 500. Hence, this model was revised by Lopez de Bertodano (1999), where it was proposed that C_{TD} be expressed as a function of turbulent Stokes number as follows:

$$C_{TD} = C_\mu^{1/4}\frac{1}{St(1+St)} \tag{38}$$

The 2-phase version of the FAD model (27) may be expressed in the same form as the Lopez de Bertodano model (37), by substituting the formula for eddy viscosity, $\nu_{t\alpha} = C_\mu k_\alpha^2/\varepsilon_\alpha$ into (27). We find that the two models are equivalent, with the adjustable 'constants' related as follows:

$$C_{TD} = \frac{C_\mu}{\sigma_{r\alpha}}\frac{\overline{C_{\alpha\beta}}}{\rho_\alpha}\frac{k_\alpha}{\varepsilon_\alpha}\left(\frac{1}{\overline{\overline{r_\alpha}}}+\frac{1}{\overline{\overline{r_\beta}}}\right) = \frac{C_\mu}{0.41\sigma_{r\alpha}}\frac{1}{St}\left(\frac{\bar{r}_\beta}{\bar{r}_\alpha}+1\right) \tag{39}$$

Hence, the FAD+EVH model for dispersed two-phase flow (27) is equivalent to a Lopez de Bertodano model with Stokes number dependent coefficient C_{TD}. However, the Stokes number dependency is not the same as that proposed by Lopez de Bertodano (1998).

Carrica Model

The model of Carrica et al (1999) was developed for dilute poly-dispersed bubbly flow, for bubbles sufficiently small that the Stokes drag law could be applied, $C_D = 24/\mathrm{Re}_\beta$. Denoting the continuous phase by $\alpha = 1$, and the dispersed phases by $\beta = 2,\ldots,ND$, the model takes the form:

$$\vec{M}_\beta^{TD} = -\frac{3}{4} C_D \frac{\bar{r}_\beta \rho_\alpha}{d_\beta} \left|\vec{U}_\beta - \vec{U}_\alpha\right| \frac{\nu_{t\alpha}}{\sigma_{r\alpha}} \nabla \bar{r}_\beta , \qquad \beta = 2,\ldots,ND \tag{40}$$

$$\vec{M}_\alpha^{TD} = -\sum_{\beta=2}^{ND} \vec{M}_\beta^{TD} \tag{41}$$

The Carrica model was evaluated in some detail by Moraga et al., 2001, 2003. Satisfactory agreement was found with DNS data for dilute bubbly flows, and for a bubbly mixing layer. Moraga et al. also noted the equivalence between this model and a variable coefficient Lopez de Bertodano model.

Comparing the Carrica model equations (40) and (41) with the FAD+EDH model equations (28) and (29 for 2-phase flow, we see that they are identical in the limit $r_\beta \to 0$. So the FAD model reduces to the model of Carrica et al. in the case of 2-phase flow, for small dispersed phase volume fractions and for small particle diameters. Consequently, the FAD model may be considered to be a generalization of the Carrica model, valid for larger dispersed phase volume fractions, and for general drag laws.

Note that the poly-dispersed forms of the FAD and Carrica model differ in their use of volume fraction gradients. The Carrica model assumes that the total turbulent dispersion force acting on each dispersed phase is proportional to the volume fraction gradient of that phase only. The FAD+EDH model for poly-dispersed flow (26) has equal and opposite contributions for each continuous-dispersed phase pair, proportional to a difference of volume fraction gradients.

5. Validation

In section 4, it has been shown that the FAD model is equivalent to several other models in the literature, in the limit of low dispersed phase volume fraction. Hence, all validation work reported for these models is also applicable to the FAD model. Here we present two further validation exercises, one for liquid-solid flows, and another for bubbly flows. All simulations have been performed using user-fortran implementations of the FAD Model in the commercial CFD package CFX-5.6 (2003).

Both validation exercises employed either the standard k-ε model, or the Shear Stress Transport (SST) turbulence model (Menter 1994) for the continuous phase. Particle induced turbulence was accounted for following the enhanced eddy viscosity model of Sato et al, 1975 and 1981. The dispersed phase turbulence was treated assuming a simple algebraic relationship between the dispersed phase and continuous phase kinematic eddy viscosities:

$$\nu_{t\beta} = \frac{\nu_{t\alpha}}{\sigma_{\nu\beta}} \tag{42}$$

where the eddy viscosity Prandtl number $\sigma_{\nu\beta}$ was set equal to unity. Also, the turbulent Prandtl number for volume fraction, $\sigma_{r\alpha}$, was set equal to unity in all calculations.

5.1 Validation for bubbly flows in a vertical pipe

Experimental set up and test case definitions

The validation of the FAD model for gas-liquid flows was based on the Forschungszentrum Rossendorf (FZR) wiremesh sensor measurement database for upward air-water flows in a vertical pipe established at the MT-Loop test facility. The primary purpose of this experiment is to permit the validation of models for interfacial forces implemented in CFD codes.

As is illustrated in Fig. 5.1(a), the test section is 4 m long and has an inner diameter 51.2 mm. The Loop was operated under atmospheric pressure and a constant temperature of 30C. Measurements were carried out for stationary flows of various air-water superficial velocity ratios at 10 different cross sections located between L/ D = 0.6 and 59.2 from the gas injection using a wiremesh sensor with 24 x 24 electrodes. Careful measures were taken to ensure axial-symmetry of the macroscopic flow. Details about the experimental set up and data accuracy are provided in Prasser et al., 2003. For the present validation we defined a number of test cases in the bubbly flow regime with wall gas peak and compared the numerical results obtained using the FAD and RPI models against the measurement data at the top measurement cross section L/D = 59.2. Numerical experiments (Shi et al., 2004) showed that the gas concentration distribution at this cross section is independent of the inlet velocity and gas volume fraction profile. The test cases, together with the inlet superficial velocities of both phases corresponding to the normal condition and the mean bubble diameter measured at L/ D = 59.2, needed as input parameters for the numerical simulation, are listed in Fig. 5.1(a).

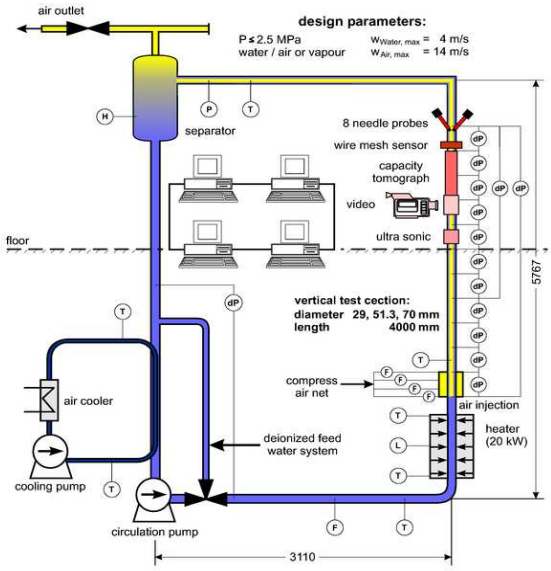

Test	d_p [mm]	$U_{l,\mathrm{sup}}$ [m/s]	$U_{g,\mathrm{sup}}$ [m/s]
017	4.8	0.405	0.0040
019	4.8	1.017	0.0040
038	4.3	0.225	0.0096
039	4.5	0.405	0.0096
040	4.6	0.641	0.0096
041	4.5	1.017	0.0096
042	3.6	1.611	0.0096
074	4.5	1.017	0.0368

Fig. 5.1(a) MT-Loop Test facility and a list of test cases.

Numerical settings

The numerical simulation was based on the CFX two-fluid model. Both fluids were assumed to be incompressible and the bubble diameter was assumed to be constant within the total computational domain. The interfacial forces are considered by the following models, the Grace model for the drag force (Grace and Weber, 1982), the Tomiyama correlations for the lift and wall lubrication force, (Tomiyama et al 1995, 1998), and either the FAD or the RPI model for the turbulence dispersion force. Here, the 'RPI model' refers to the constant coefficient Lopez de Bertodano model, eq. (37). The added mass force was neglected for the stationary flow considered here.

A detailed discussion on the lift and lubrication forces is given in Shi at al 2004. Here, we concentrate on comparisons between the turbulence dispersion models. Shi et al 2004 also

considered comparisons of both the *k-ε* and SST turbulence models. It was concluded there that the SST model yielded superior predictions to the *k-ε* model. All comparisons here employ the SST model.

A computational domain consisting of a 3 degree sector of the pipe with the symmetry condition on both sector faces was applied in the simulation. A uniform volume fraction distribution was assumed for both phases at the inlet together with a 1/7-th power inlet velocity profile, $U_{in} = 1.224 U_0 \left(1 - r^*\right)^{1/7}$, where U_0 is the mean value, for the liquid, and a uniform profile for the gas phase. The radial velocity was assumed to be null. In addition, a medium turbulence intensity (5%) was assigned there. The outlet was located at 3.3m away from the inlet, where an averaged static pressure equal to the atmospheric pressure P_0 was assigned. The pressure field was initialized using the expression $P = P_0 + \rho_l \left| g(3.3 - L) \right|$. Details on the convergence error, grid dependence of the results and the inlet condition effect are reported in Shi et al (2004).

Evaluation and discussion

Calculation was carried out using the FAD and the RPI model for the turbulence dispersion force, respectively. The results for the normalized air volume fraction, which is defined by equation (43), were compared at the cross section chosen for validation, L/D = 59.2.

$$\alpha_g^* = \frac{\alpha_g}{\alpha_{g,0}}, \text{ with } \quad \alpha_{g,0} = 2\int_0^1 \alpha_g \left(r^*\right) r^* dr^* \tag{43}$$

Computational results are displayed in Fig. 5.1(b), together with the corresponding measurement data. It can be observed that all numerical results based on the FAD model agree fairly well with the experimental data. It is observed from Fig. 5.1(b) that the gas volume fraction obtained using the RPI model is consistently lower in the core region than those based on the FAD model. This indicates a stronger turbulence dispersion force given by the latter. The difference of the results is not essential in all cases. Nevertheless, the FAD model leads to much better agreements with the experimental data in certain cases, such as FZR-074, though the core gas concentration is still underpredicted. This deviation can be reduced by using two fluids for the gas phase, namely separating the larger bubbles (negative lift force) from the small ones. This will be the subject of future investigation.

Similar to the observation to FZR-074 and FZR-042, the RPI model overpredicted the wall gas peak, and at the same time underpredicted the core gas concentration in all cases. In order to make a direct comparison for both models, the corresponding turbulence dispersion force coefficient of the FAD model was estimated for all test cases using eq. (39) and is plotted in Fig. 5.1(c) together with a constant coefficient C_{TD} = 0.35 used in the RPI model. The results clearly show that the turbulence dispersion force given by the RPI model is much too weak, except in the near-wall region. Moreover, Fig. 5.1(c) also shows that a constant coefficient C_{TD} as assumed in the RPI model is not realistic. Due to this oversimplification, the RPI model does not take a number of physical dependencies appearing in eq. (39) into account. In addition, it is interesting to note that C_{TD} decreases with increasing superficial velocity of the continuous phase. This is because the bubble response time τ_d is similar for all test cases due to their similar d_p, whereas the turbulence time scale τ_t decreases with increasing flow Reynolds numbers.

Despite the acceptable agreements between numerical results and measurements achieved using the above non-drag force models, it is necessary to address the limitation of the present study. First, bubble coalescence and breakup was neglected in this investigation. Larger bubbles which receive a negative lift force were also not distinguished from small bubbles. This might be the main reason responsible for the deviations observed in the core region. In addition, the numerical results indicate a bubble free region in the wall proximity, which is

different from the experimental data. A number of causes can have contributed to this deviation, e.g., the decreased measurement accuracy in the wall proximity and the inaccuracy of the wall lubrication force models.

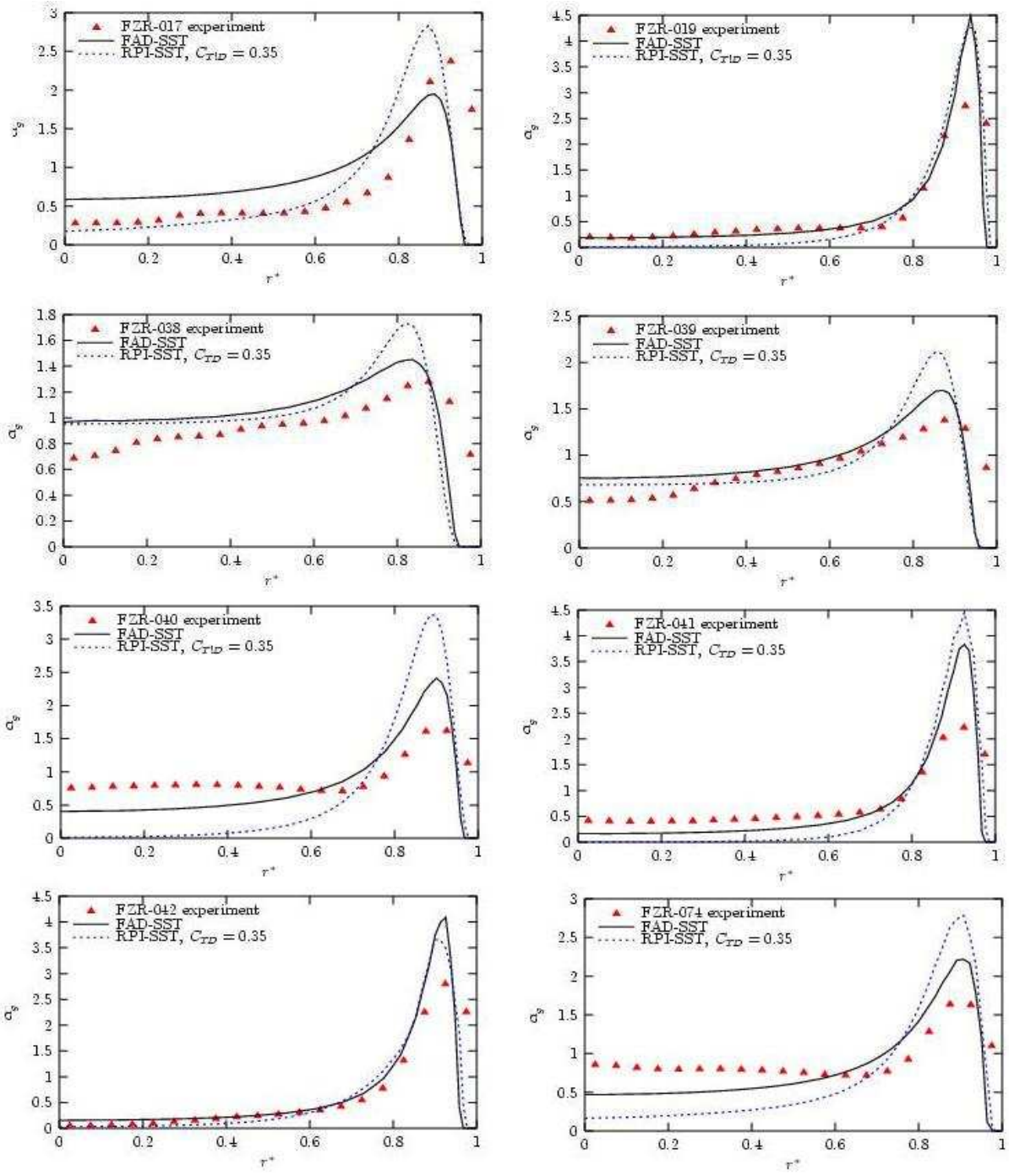

Fig. 5.1 (b) Comparisons between the RPI and FAD model.

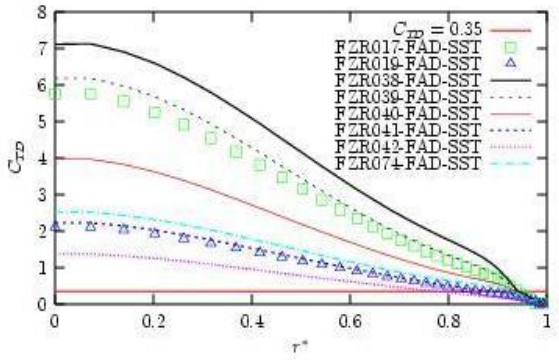

Fig. 5.1(c) Equivalent C_{TD} coefficient of FAD model in comparison with RPI Model.

5.2 Liquid-Solid Flows in Mixing Vessels

CFD results are presented for one of the experimental cases investigated by Micheletti 2003. The system comprises a single six-blade Rushton disc turbine in a cylindrical mixing vessel of diameter, T, and height, H, 290mm, with four wall-mounted full-length baffles of radial extent T/10. Details of the specific case which is simulated are:

- Impeller clearance - C=0.33T
- Impeller speed - 800rpm
- Particles - glass ballotini, diameter 600-710μm, average volume fraction C_{av}=5.5%
- Continuous-phase fluid - tap water

The CFX simulation uses the following set-up:

- Wen Yu (1966) correlation for interphase drag coefficient. This model employs the standard Schiller-Naumann drag model with volume fraction corrections to account for hindered settling effects
- FAD model for turbulent dispersion.
- SST turbulence model (Menter 1994) for the continuous phase, enhanced by Sato and Sekoguchi 1975 model for particle-induced turbulence.
- Dispersed-phase zero-equation turbulence model for the particle phase.
- High Resolution differencing on all equations
- Hexahedral mesh, with 211640 elements, 229565 nodes. The symmetry of the system is exploited such that only one half of the vessel is simulated.
- Steady-state Frozen Rotor model
- The vessel is modeled in the with-lid condition, with a no-slip wall used at the upper boundary.

Micheletti's experimental results are presented in terms of particle volume fractions on two vertical lines through the vessel, one at $r = 0.25T$, the other at $r = 0.45T$, located on a plane mid-way between an adjacent pair of baffles. The experimental data are obtained using a conductivity probe with 10mm square electrodes mounted 10mm apart (Micheletti et al 2003). As there is no information available from the experimental study on the size distribution of particles within the specified range of 600-710μm, simulation results are presented for mono-disperse systems at the two extremes of the size range.

The measuring location at $r = 0.25T$ lies within the rotating part of the computational domain. Since the steady-state Frozen Rotor model does not produce time-resolved results, a circumferential average of the predicted volume fraction is calculated. This is assumed to provide a fair representation of the time average of the periodic variation in volume fraction

experienced by the probe. Minimum and maximum values of the particle volume fractions within a region ±5mm from the stated data point are included. This dimension is representative of the size of the conductivity probe used in the experimental work.

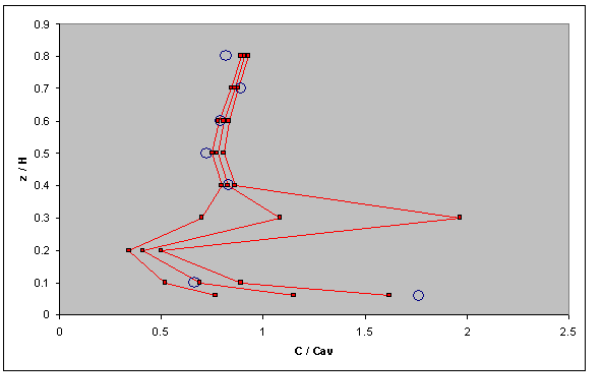

Fig. 5.2 (a) r = 0.25 T; 600 microns

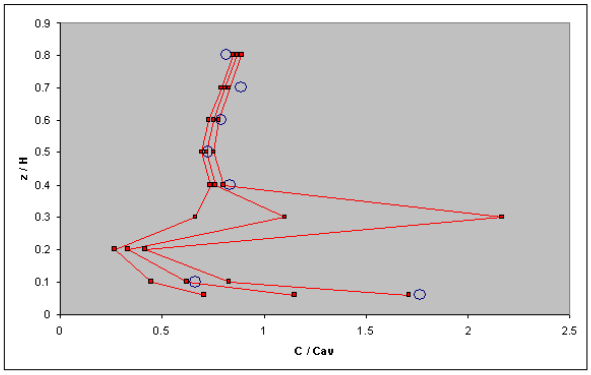

Fig. 5.2 (b) r = 0.25 T; 710 microns

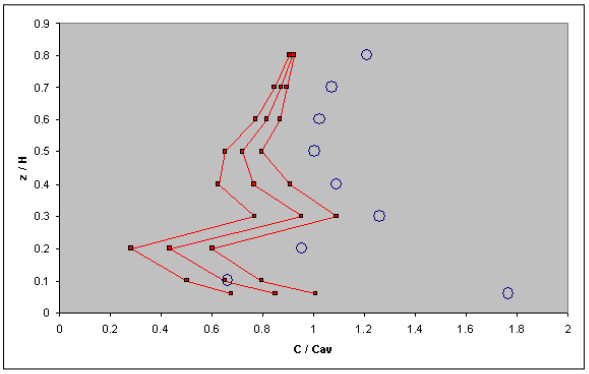

Fig. 5.2 (c) r = 0.45T; 600 microns; xy-plane

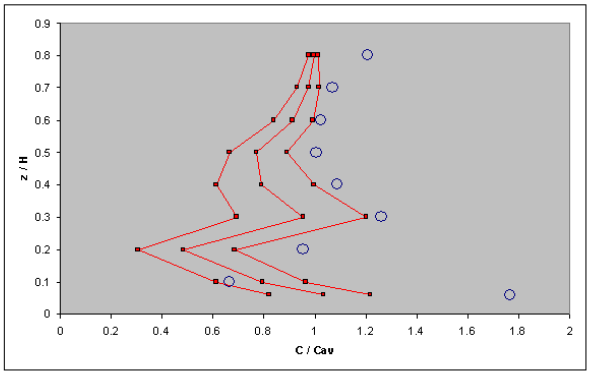

Fig. 5.2 (d) r = 0.45T; 600 microns; xz-plane

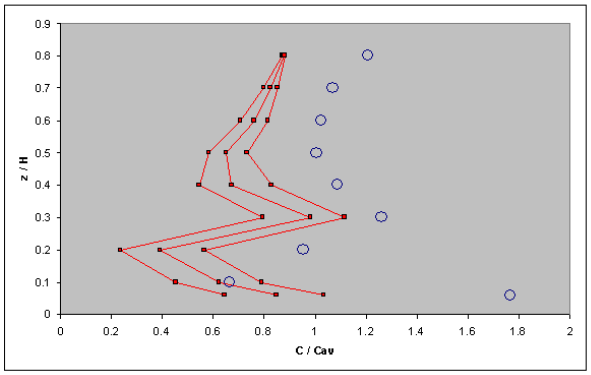

Fig. 5.2 (e) r = 0.45T; 710 microns; xy-plane

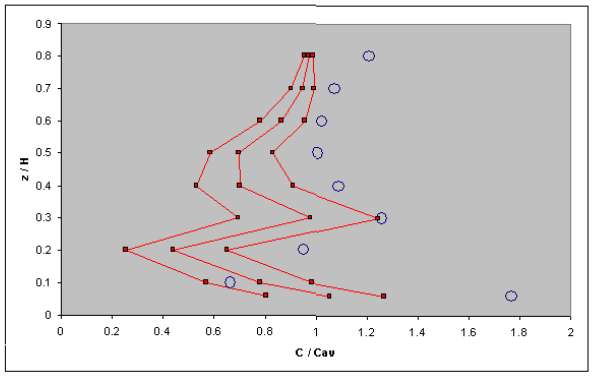

Fig. 5.2 (f) r = 0.45T; 710 microns; xz-plane

At r = 0.45T, two sets of results are presented. One set lies on an *xy*-plane, which is located mid-way between baffles and is aligned with one of the impeller blades; the other is on an *xz*-plane, which is located mid-way between baffles and passes mid-way between a pair of impeller blades. In all of the volume fraction profile graphs, the discrete points are the experimental data, whilst the three solid lines are the minimum, average and maximum values of the CFD results.

The results at r = 0.25T are presented in Figures 5.2(a) and 5.2(b) for the 600μm and 710μm particles respectively. The predictions are in good agreement with the experimental data, and indicate that the particle distribution in this region is relatively insensitive to particle size.

Figures 5.2(c) and 5.2(d) contain the results at r = 0.45T for 600μm particles plotted on the *xy*- and *xz*- planes between baffles described above. Figures 5.2(e) and 5.2(f) present the same data for the 710μm particles. The predictions here consistently under-predict the particle

volume fractions recorded experimentally, though the correct trend is predicted. It is notable that there are differences between the predicted results on the two plotting locations.

Figures 5.2(g) and 5.2(h) show contours of particle volume fraction, normalized by the mean volume fraction. Figure 11 presents the full range of values within the plane, whilst Figure 12 uses a reduced range of 0 to 3, to emphasize the detail near the walls. In the region below the impeller, the solids concentration attains a maximum value of ~60%. The CFD model does not include any solids pressure terms to account for particle-particle impacts and may therefore be expected to over-predict the solids loading in regions where sedimentation occurs. This accumulation of solids at the base of the vessel will therefore lead to a lower mean concentration in the remainder of the vessel. This may be one explanation for the lower prediction of particle volume fraction at the vessel wall.

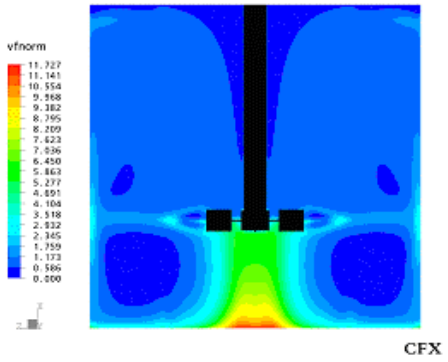

Fig. 5.2 (g) Normalised Volume Fractions

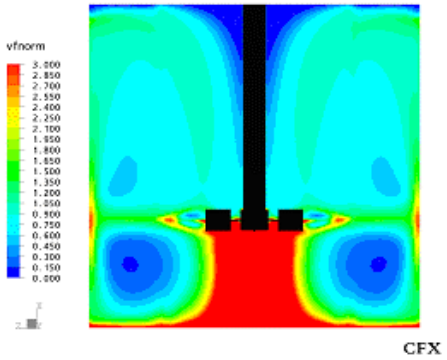

Fig. 5.2 (h) Normalised Volume Fractions (reduced range)

6. Conclusions

The Favre Averaged Drag Model has been shown to generalize most current models of turbulence dispersion, and to possess a wide degree of universality. Consequently, it has been implemented as the default model of choice for turbulence dispersion in CFX-5.7 (2004).

Many topics remain for further investigation. For example:

- The current model assumes a linear dependence of drag force on slip velocity, as far as the averaging procedure is concerned. How is the model affected by generalizing this to take into account dependence of $D_{\alpha\beta}$ (eq. 16) on slip velocity?
- Similarly, how is the model changed by taking into account volume fraction dependence of the drag coefficient, for example, power law corrections at high dispersed phase volume fractions?
- In its general form (eq. 21), the FAD model is applicable, in principal, to second order closure models for turbulence, and to separated as well as dispersed multi-phase flows.

We believe such further investigations will provide further fruitful insights into turbulent multiphase flows.

Acknowlegements

This work is the result of a strong collaboration between Forschungszentrum Rossendorf and ANSYS-CFX Germany. Financial support is gratefully acknowledged from the Ministry of Economy and Labour (BMWA) of Germany in the project "TOPFLOW – Transient two phase flow test facility for generic investigation of two-phase flows and further development and validation of CFD codes", and to ANSYS Germany GmbH in the project "Development

of CFD codes for multidimensional flows in reactor safety applications".

We are grateful to King's College, London, for kind permission to show the results of the experiment and simulations by Micheletti et al. These were performed as part of Project OPTIMUM, G1RD-CT-2000-00263, 'Optimization of Industrial Multiphase Mixing', funded by the European Community under the 'Competitive and Sustainable Growth' Program (1998-2002).

References

1. A. Behzadi, R.I. Issa, H. Rusche (2001), Effects of turbulence on inter-phase forces in dispersed flow, *ICMF 2001, 4th Int. Conf. Multiphase Flow*, New Orleans, LA, USA.
2. D.C. Besnard and F .H. Harlow (1988), Turbulence in multiphase flow, *Int. J. Multiphase Flow*, Vol. 14, p. 679.
3. P.M. Carrica, F. Bonetto, D.A. Drew, R.T. Lahey (1998), The interaction of background ocean air bubbles with a surface ship, *Int. J. Num. Meth. Fluids*, Vol. 28, p. 571.
4. P.M. Carrica, D.A. Drew, R.T. Lahey (1999), A polydisperse model for bubbly two-phase flow around a surface ship, *Int. J. Multiphase Flow*, Vol. 25, pp. 257-305.
5. C.T. Crowe (2000), On Models for Turbulence Modulation in Fluid-Particle Flows, *Int. J. Multiphase Flow*, Vol. 26, p. 719.
6. CFX-5.6 Users Manual, ANSYS, 2003.
7. CFX-5.7 Users Manual, ANSYS, 2004.
8. D.A. Drew (1983) Mathematical Modelling of Two-Phase Flows, *Ann. Review Fluid Mech.*, Vol. 15, p. 261.
9. S.E. Elghobashi and T.W. Abou-Arab (1983), A two equation turbulence model for two- phase flows, *Phys. Fluids*, Vol. 26, p. 931.
10. A.D. Gosman, C. Lekakou, S. Politis, R.I. Issa, and M.L. Looney (1992), Multidimensional Modeling of Turbulent Two-Phase Flows in Stirred Vessels, AIChEJ Vol. 38, p. 1946.
11. J. R. Grace and M. E. Weber (1982), Hydrodynamics of drops and bubbles, in Handbook of Multiphase Systems, ed. G. Hetsroni, Hemisphere.
12. K. Johansson, A. Magnesson, R. Rundqvist and A.E. Almstedt (2001), Study of two gas-particle flows using Eulerian/Eulerian and two-fluid models, *ICMF 2001, 4th Int. Conf. Multiphase Flow*, New Orleans, LA, USA.
13. B. Kashiwa and W.B. VanderHeyden (2000), Towards a General Theory for Multiphase Turbulence Part I: Development and Gauging of the Model Equations, Los Alamos National Laboratory Report LA-13773-MS.
14. I. Kataoka (1986), Local instant formulation of two-phase flow, *Int. J. Multiphase Flow*, Vol. 12, p. 745.
15. I. Kataoka and A. Serizawa (1989), Basic equations of turbulence in gas-liquid two-phase flow, *Int. J. Multiphase Flow*, Vol. 15, p. 843
16. E. Krepper, H.M. Prasser (2000), Measurements and CFX-Simulations of a bubbly flow in a vertical pipe, *AMIF-ESF Workshop "Computing Methods for Two-Phase Flow"*, Aussois, France.
17. C. Ljus (2000), On particle transport and turbulence modification in air-particle flows, Ph. D. Thesis, Chalmers University of Technology, Sweden.

18. M. Lopez de Bertodano, (1992), Turbulent bubbly two-phase flow in a triangular duct, Ph. D. Thesis, Rensselaer Polytechnic Institute, New York, USA.

19. M. Lopez de Bertodano, R. T. Lahey and 0. C. Jones (1994a), Development of a k-e model for bubbly two-phase flow, *Trans. ASME J. Fluids Eng*, Vol. 116, p. 128.

20. M. Lopez de Bertodano, R. T. Lahey and 0. C. Jones (1994b), Phase distribution in bubbly two-phase flow in vertical ducts, *Int. J. Multiphase Flow*, Vol. 20, p. 805

21. M. Lopez de Bertodano, (1998), Two fluid model for two-phase turbulent jet, *Nucl. Eng. Des.* Vol 179, p. 65.

22. D. Lucas, E. Krepper, H.-M. Prasser (2001), Development of bubble size distributions in vertical pipe flow by consideration of radial gas fraction profiles, *ICMF 2001, 4th Int. Conf. Multiphase Flow*, New Orleans, LA, USA.

23. F.R. Menter (1994), Two-equation eddy-viscosity turbulence models for engineering applications, *AIAA-Journal*, Vol. 32, No. 8.

24. F.R. Menter (2002), *CFD Best Practice Guidelines (BPG) for CFD code validation for reactor safety applications*, EC Project ECORA, Report EVOL-ECORA-D01.

25. M, Micheletti (2002), Solid concentration measurements in stirred vessels – Part 2.

26. M. Micheletti, L. Nikiforaki, K.C. Lee, and M. Yianneskis (2003), 'Particle Concentration and Mixing Characteristics of Moderate to Dense Solid-Liquid Suspensions', *Industrial and Engineering Chemistry Research*, Vol. 42, p. 6236.

27. F.J. Moraga, A.E. Larreteguy, D.A. Drew, R.T. Lahey (2001), Assessment of turbulent dispersion models for bubbly, *ICMF 2001, 4th Int. Conf. Multiphase Flow*, New Orleans, LA, USA.

28. F.J. Moraga, A.E. Larreteguy, D.A. Drew, R.T. Lahey (2003), Assessment of turbulent dispersion models for bubbly flows in the low Stokes number limit, *Int. J. Multiphase Flow*, Vol. 29, p. 655.

29. H.-M. Prasser, D. Lucas, E. Krepper, D. Baldauf (2003), A. Böttger, U. Rohde et.al, *Strömungskarten und Modelle für transiente Zweiphasenströmungen*, Forschungs-zentrum Rossendorf, Germany, Report No. FZR-379, June 2003.

30. Y. Sato, K. Sekoguchi (1975), Liquid velocity distribution in two phase bubble flow, *Int. J. Multiphase Flow*, Vol. 2, p. 79.

31. Y. Sato, M. Sadatomi and K. Sekoguchi (1981), Momentum and heat transfer in two phase bubble flow, *Int. J. Multiphase Flow*, Vol. 7, p. 167.

32. Serizawa and I. Kataoka (1990), Turbulence suppression in bubbly two-phase flow, *Nucl. Eng. Design*, Vol. 122, p.1.

33. J.-M. Shi, Th. Frank, E. Krepper, D. Lucas, U. Rhode, and H.-M. Prasser, Implementation and Validation of Non-Drag Interfacial Forces in CFX-5.6, *ICMF 2004, 5th Int. Conf. Multiphase Flow*, Yokohama, Japan.

34. A. Tomiyama, A. Sou, I. Zun, N. Kanami, and T. Sakaguchi (1995), Effect of Eotvos number and dimensionless liquid volumetric flux on lateral motion of a bubble in a laminar duct flow, *Advances in Multiphase Flow*, p. 3-5, Elsevier Science.

35. A. Tomiyama, (1998), Struggle with computational bubble dynamics, *ICMF'98, 3rd Int. Conf. Multiphase Flow*, Lyon, France.

36. C.Y. Wen and Y.H. Yu (1966), Mechanics of fluidisation, *Chem. Eng. Prog. Symp. Series*, Vol. 62, p. 100